Int. J. Heat Mass Transfer. Vol. 27, No. 11, pp. 1985–1998, 1984
Printed in Great Britain

0017–9310/84 $3.00 + 0.00
Pergamon Press Ltd.

Physical behaviour of electron-beam fusion heat transfer and deep penetration in metals

T. VIJAYAN and V. K. ROHATGI
Plasma Physics Division, Bhabha Atomic Research Centre, Trombay, Bombay 400085, India

(*Received* 11 *March* 1982 *and in revised form* 15 *November* 1983)

Abstract—A simple model of fusion and deep penetration in metals under electron-beam interactions and energy transfer, is described in this paper. In this model, electrons in the beam penetrate a depth S and cause melting there, during which thermal-conduction melting occurs in a further depth z_i in the beam direction. Hence, in the first discretized-fusion step, fusion depth $D_1 = S + z_1$, and total fusion depth in j steps, $h = \sum_{i=1}^{j} (S + z_i)$. Also, thermal conduction from a line source from the surface to the cavity bottom, causes sideways melting. In general, thermal-conduction melting f is given as

$$f = \left[\frac{f_0 q_0 V'}{4\pi^2 x_0 T_m} \exp(-R_0^2/k_0 t)\right]$$

where, f_0 is a dimensionless variable dependent on the beam and metal, q_0 and V' are source-strength and source-travel parameters, x_0 is a unit distance, T_m is the melting point, R_0 is a distance variable, $k_0 = K/\rho c$ is the thermal diffusivity, K is the coefficient of thermal conductivity, ρ is the metal density and c is the specific heat. The sideways melting in succeeding steps add up to the initial melt width, to give the final width. Also, for metals $K > K_0 (= 100\ \mathrm{J\ m^{-1}\ K^{-1}\ s^{-1}})$, meltings z_i and f are reduced by $(K_0/K)^{1/2}$, due to large-scale thermal losses outwards. Using the present model, fusion profiles and penetrations for various conditions of the beam and metals were investigated through numerical calculation and are validated through experiments.

1. INTRODUCTION

FUSION by an electron beam is finding applications in numerous fields of a specialized nature. These fields include material refining, joining, intense evaporation, ablation, etc, through beam fusion which fulfils various material, metallurgical and energy conservation requirements in general. As a matter of fact, great strides have already been made in the experimental developments using electron beams. Also, the results from experiments have been overwhelmingly rewarding. In spite of these, a complete theoretical understanding of beam fusion mechanisms, especially concerning deep penetration, is still lacking. In this context, a qualitative picture of beam fusion alone has been offered by Schwarz [1], a detailed study of the steady-state effects is provided by Swift-Hook and Gick [2], a detailed physical description of the steady state but in a semi-quantitative manner, is given by Klemens [3], and steady-state key-hole profiles especially for rapid boiling, and the surface tension effects on deep penetration, are described by Andrews and Atthey [4]. As such, it can be seen that there is no published work which contains a detailed picture of all the aspects taken together, and including the transient effects. In this context, as far as Stefan problems in moving surface-point sources are concerned [5], a good number of works can be found in the literature, whereas, deep fusion by an electron beam is better represented as a line source. In this case, an exact solution in complete detail, has been found to be extremely complicated due to the presence of various nonlinearities [6] encountered in the process. In view of this, a finite-difference method [7] also could not be followed. Whereas, in this study, we have attempted to include the details of various aspects of deep-penetration fusion together, through approximations and penetrations in discrete steps.

The aim of the present work is to describe the physical nature of transient fusion and deep penetration by an electron beam in semi-infinite metal targets. Here, the models cited above are for steady-state fusion and for beam deposition in a steady-state key-hole. Whereas the present work studies transient fusion and transient formation of key-hole, starting from the beam-on stage and leading to the steady state. For this purpose, a method of fusion penetration in discrete steps and superposing the various effects, to give a complete description of fusion, have been evolved here. This model has been applied to numerical computations which are of considerable practical importance in beam-welding applications. The predictions from these calculations, are in conformity with observed results, both from this study as well as from the literature [1, 2].

2. BEAM-FUSION MODEL

Energy dissipation [8] by electrons in a solid is defined by Bethe's continuous slow-down approximation [9]. Also, using the Thomson–Whiddington law, the electron penetration range S in a target can be written as

$$S = aAE^2/\rho Z \qquad (1)$$

where, a is a constant, E is electron energy and A, ρ and Z are atomic weight, target density and atomic number,

NOMENCLATURE

a	constant [kg^{-1} m^{-6} s^4]
A_0	source strength [J m^{-3} s^{-1}]
A	atomic weight
c	specific heat [J kg^{-1} K^{-1}]
c_e	c parameter [J]
D_i	$S+z_i$ [m]
d	beam spot width [m]
E	electron energy [J]
e	electronic charge [C]
F	isothermal advance in general [m]
F_i	isothermal advance in time t_i [m]
f	isothermal advance or fusion growth in time t_i in the case of melting [m]
f_0	$[K_e/(c_e+L_e)(r_0/S)]^{1/2}$
g	acceleration due to gravity [m s^{-2}]
H	heat input, $\sum_{i=1}^{j} H_D(i)+\sum_{i=1}^{j} H_i$ [J]
$H_D(i)$	heat to melt thickness D_i [J]
H_i	heat used for growths f all along the fusion profile in the ith step, $\sum_{l=1}^{i} Q_{(i,l)}$ [J]
$H(i)$	heat needed for ith step, $H_D(i)+H_i$ [J]
h	fusion depth, $\sum_{i=1}^{j} D_i$ [m]
I	electron beam current density [A m^{-2}]
i	penetration step number
j	total penetration steps
K	coefficient of thermal conductivity [J m^{-1} K^{-1} s^{-1}]
K_0	thermal conductivity limit, 100 J m^{-1} K^{-1} s^{-1}
K_e	K parameter [J]
k	step numbers describing the fusion width at any particular step number
k_B	Boltzmann constant [J K^{-1}]
k_0	coefficient of thermal diffusivity, $K/\rho c$ [m^2 s^{-1}]
L_e	L_m parameter [J]
L_m	latent heat of fusion [J kg^{-1}]
L_v	latent heat of evaporation [J kg^{-1}]
l	growth number
m_a	atomic mass [kg]
m	electron mass [kg]
m_0	evaporating mass rate per unit area [kg m^{-2} s^{-1}]
P_v	vapour pressure [Pa]
Q	beam energy input in time t', Wt' [J]
Q_0	source strength parameter [K m^2]
$Q_{(i,l)}$	heat for growths $x_{(i,l)}$ and $y_{(i,l)}$ [J]
q	heat content for melting $\rho[c(T_m-T_0)+L_m]$ [J]
q_m	heat content in melt, $q+\rho c\,(T-T_m)$ [J]
q_0	intense source strength parameter [K m^2]
R_0	distance, $\beta_0 R_i$, [m]
R_i	distance of interface [m]
r	radius of curvature of the cavity [m]
r_0	beam spot half width [m]
S	electron residual range [m]
T	temperature in general [K]
T_0	ambient temperature [K]
T_m	melting point [K]
T_B	boiling point [K]
t	time [s]
t_i	time to complete step i [s]
t'	traverse time interval [s]
t_0	time to melt volume ψ [s]
V	travel speed [m s^{-1}]
V'	speed parameter [m]
v	electron velocity [m s^{-1}]
W	beam power [J s^{-1}]
$X_{(i,k)}$	interface distance in x-direction [m]
x_0	unit distance [m]
$x_{(i,l)}$	growth f in the x-direction [m]
$Y_{(i,k)}$	interface distance in y-direction [m]
$y_{(i,l)}$	growth in y-direction [m]
Z	atomic number
z_i	growth in z-direction [m].

Greek symbols

β_0	$[(r_0/x_0)(1+\cos\phi)]^{-1/2}$
γ_0	melt fraction
σ_0	surface tension at T_m [N m^{-1}]
σ_T	surface tension at T [N m^{-1}]
ρ	metal density [kg m^{-3}]
ρ_m	melt denstiy at T_m [kg m^{-3}]
ρ_T	melt density at T [kg m^{-3}]
ψ	volume, $\pi r_0^2 S$ [m^3]
ϕ	beam angle [deg.].

respectively. Using these concepts, the nature of electron-beam fusion and deep-penetration effects are determined in the present study for the normal incidence of a beam in a simple model which is illustrated in Fig. 1(a). In this model, beam penetration is taking place in discrete steps (i) of layer thickness D_i [see Fig. 1(b)] which is made up of the electron range S and a melt growth thickness z_i due to thermal conduction which takes place in the direction of the beam in a time interval t_i

$$D_i = S+z_i. \tag{2}$$

When the beam is just turned on a metal, heating and fusion will be initiated in a thickness S of the metal in a time t_0. However, melting grows further into the metal due to thermal conduction, and hence heating in the first step continues beyond the time interval t_0. Also, as more and more heat is deposited by the beam in this

region, it tends to raise the melt temperature, whereby vapour pressure kinetics [3, 6, 10, 11] come into play over the melt surface. This pressure (P_v) as it increases, pushes the melt sideways and generates a cavity in the melt in the path of the beam. Here, pressure balancing inside the cavity is written as

$$P_v + \frac{I}{e} mv + m_0 \left[\frac{k_B T}{m_a}\right]^{1/2} = \frac{\sigma_T}{r} + h\rho_T g \qquad (3)$$

where, I is electron current density; e, m, and v are electron charge, mass, and velocity, respectively; m_0 is the evaporation rate density; k_B is Boltzmann's constant; m_a is the atomic mass; σ_T is the surface tension at temperature T; r is the radius of curvature in the cavity; h is the cavity depth; ρ_T is the melt density at T; and g is the acceleration due to gravity.

Using equation (3), it is shown in Table 1 that recoil pressure at a temperature near to the melting points of metals in general is small (only a few Pascals). However, this pressure can be of a high magnitude at temperature greater than the boiling point [4] which is not meant in this study. Whereas Table 1 reveals that vapour pressure is playing a major role in the generation of cavities of depth cited here.

As the pressure P_v in the cavity further increases, the cavity base steadily moves down towards the melt bottom, and in time t_1 the cavity base meets the solid region below. Hence from now onwards, the beam is available to deposit heat in next step, namely, D_2 and then in D_3, and so on. In this manner, fusion continues and the cavity develops into a key-role and deep penetration results. The total penetration h after j steps in this case is written as

$$h = \sum_{i=1}^{j} D_i. \qquad (4)$$

In this case, the speed of penetration will be an inverse function of $\sum_i t_i$.

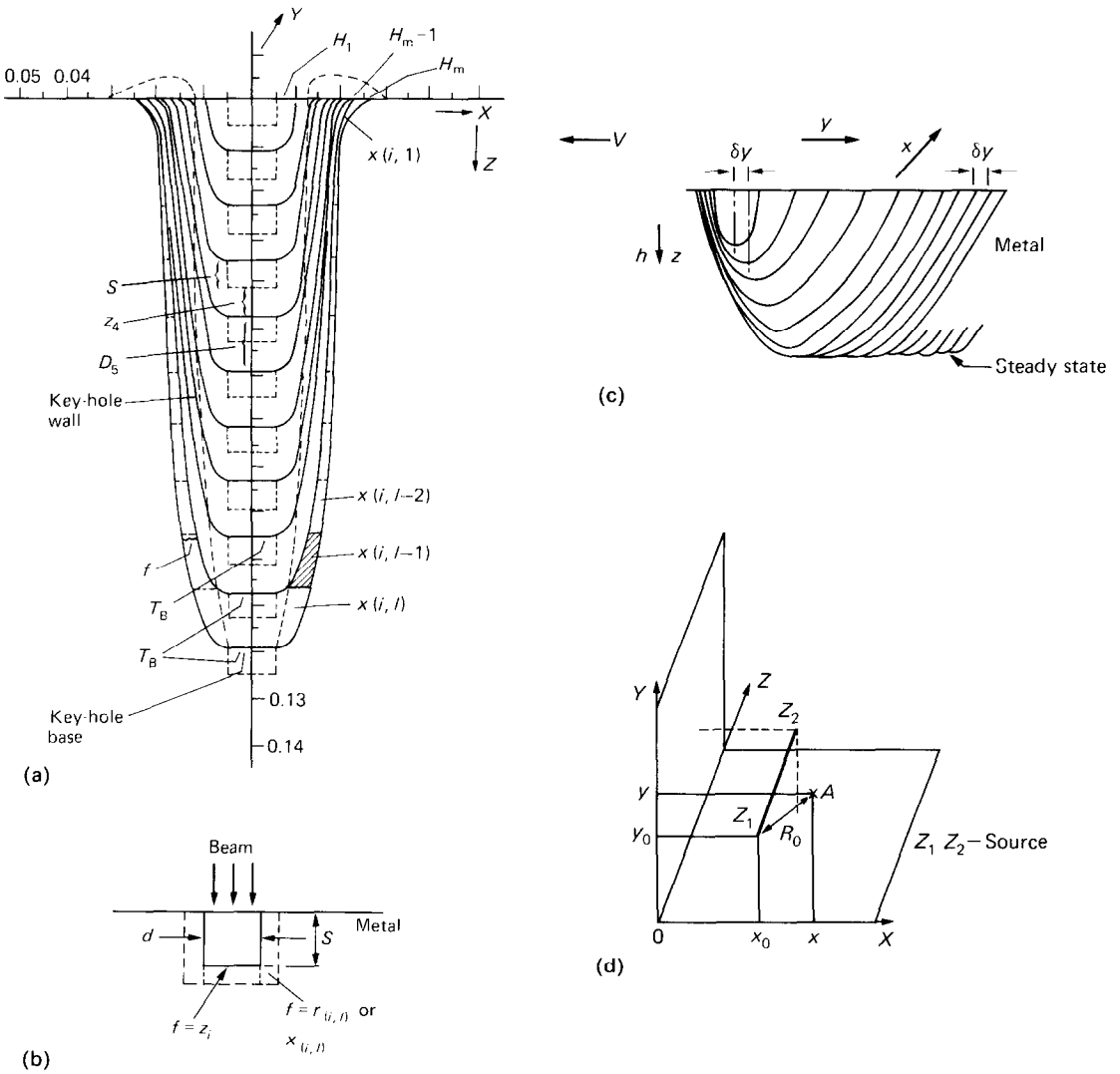

FIG. 1. (a)–(d).

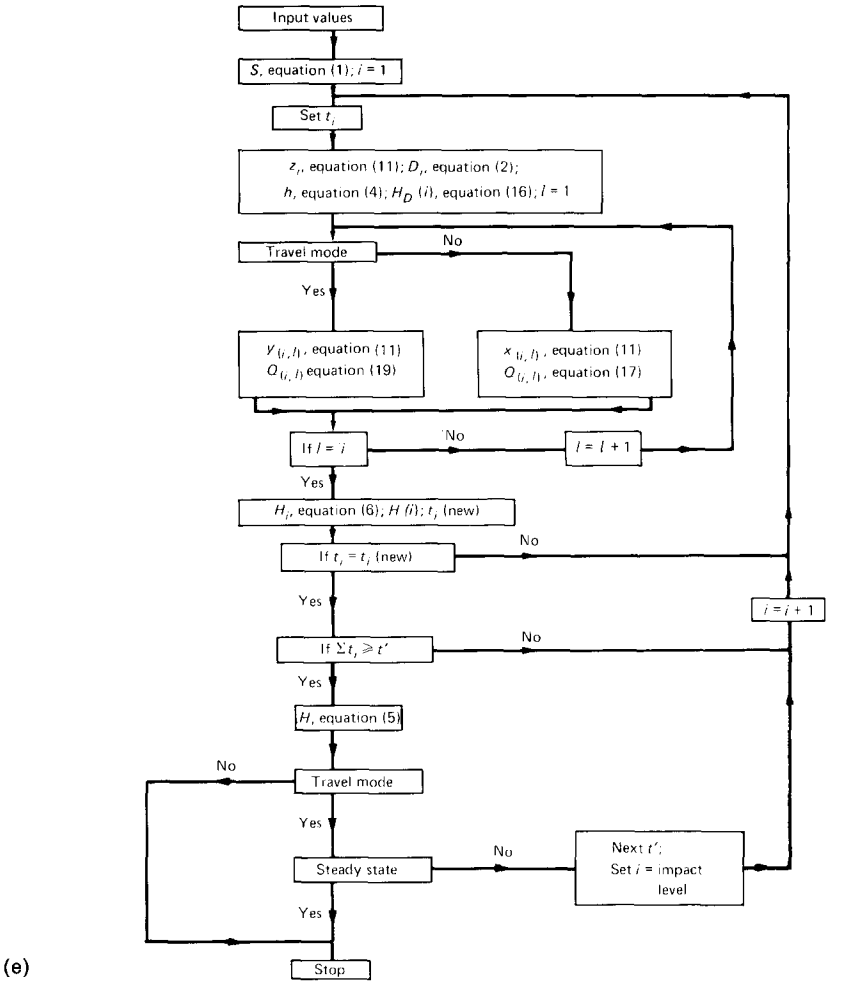

FIG. 1. (a) Schematic of the beam-fusion model. (b) Melt growth layer model. (c) Fusion-penetration development during source travel (schematic). (d) Line source concept in metal. (e) Flow chart of computation scheme.

Here, instead of an exact model, a simple model to describe interactions of a continuous beam has been employed for the reasons cited above. Whereas, though the beam is broken up in discrete steps in this model, these steps are in effect treated here in a complete succession of events, wherein, accumulated effects from the succeeding steps, are also adequately included in a continuous fashion. In this, the melting-point isothermal in the Z-direction is determined through a heat balance along the axis of the key-hole over the electronic penetration, and a further heat spread through thermal conduction. That is, $h = \sum_i (S + z_i)$ gives the position of the isothermal in i steps in the Z-direction. Whereas the advance of this isothermal

Table 1. A comparison of pressures acting in key-hole in deep penetration ($\pi r_0^2 m_0 \simeq 10^{-10}$ kg s^{-1}; $r_0 = 1 \times 10^{-4}$ m; $E = 150$ keV; $I \simeq 3 \times 10^5$ A m^{-2})

Metal	Hole depth h (mm)	Temperature at hole base T (K)	P_v (Pa)	$\frac{I}{e}mv$ (Pa)	$m_0\left[\frac{k_B T}{m_a}\right]^{1/2}$ (Pa)	$\frac{\sigma_T}{r}$ (Pa)	$h\rho_T g$ (Pa)
Al	1	2150	3817.3	446.6	2.58	4244	22.52
	50	2185	4789.8	446.6	2.6	4137	1102
Cu	1	2293	9559.9	446.6	1.74	9932	76.27
	50	2448	13 191.6	446.6	1.8	9832	3808
Fe	1	2680	12 188.3	446.6	2.0	12 570	66.92
	50	2722	15 226.4	446.6	2.02	12 400	3275

sideways is found by considering lateral heat conduction from the melt. Also, these advances during successive time steps add up to give the final boundary of the isothermal in this region. As a matter of fact, this model is as good as a continuous beam model in all respects. In these cases and also in Z-melting by heat conduction; for the coefficient of thermal conductivity $K < K_0$ ($= 100$ J m^{-1} K^{-1} s^{-1}), fusion extends up to the melting-point isothermal boundary; while for $K > K_0$, fusion does not extend up to this boundary. In general, energy H necessary to melt the metal in depth h is obtained as

$$H = \sum_{i=1}^{j} H_D(i) + \sum_{i=1}^{j} H_i \tag{5}$$

where $H_D(i)$ is the heat necessary in thickness D_i of the beam impact area; and H_i is the heat for isothermal growth by thermal conduction in the transverse plane and over the complete melt depth, which is occurring during any single interval t_i, and is given as

$$H_i = \sum_{l=1}^{i} Q_{(i,l)} \tag{6}$$

where l represents all the earlier step numbers to denote melt growths $x_{(i,l)}$ and $y_{(i,l)}$ over the full depth in time step t_i [Fig. 1(a)] and $Q_{(i,l)}$ is the heat necessary for these growths. In this case, the value of H_i tends to increase with step i. Hence, the energy parameter $H(i)$ [$= H_D(i) + H_i$] which is necessary for completion of any step i, also increases with i. This means, time $t_i = H(i)/W$, where W is the beam power, increases with step i, and hence the speed of penetration decreases with i in general. The case of fusion during source travel with speed V in the transverse direction, is illustrated in Fig. 1(c). Here, the source is assumed to be moving in steps of a travel distance δy which is equal to the beam spot width d. Also, it is assumed that the beam is stationary at a given step δy for a time interval t' which is equal to $[d/V]$.

3. FUSION-SPREAD THEORY

In general, heat conduction in metals obeys an exponential law [12] for the geometry under consideration. Whereas, during fusion of metals also similar heat transport is expected and melt grows to its neighbourhood through thermal conduction. Here in the present study, theoretical expressions to determine fusion spreading through thermal conduction, were derived using these concepts.

The Poisson heat flow for the transient case in the present problem is described by the following differential equation stated in two-dimensional coordinates

$$\frac{\delta^2 T}{\delta x^2} + \frac{\delta^2 T}{\delta y^2} - \frac{1}{k_0}\frac{\delta T}{\delta t} = -\frac{A_0}{K} \tag{7}$$

where T is the temperature, A_0 the source strength, $k_0 = K/\rho c$, is the thermal diffusivity, c is the specific heat, and K is assumed to be constant here for simplicity. This equation when solved for an instantaneous line source consideration, T is written as [12]

$$T = \frac{Q_0}{4\pi k_0 t}\exp(-R_0^2/4k_0 t) \tag{8}$$

where Q_0 is the source strength parameter for line source, $R_0^2 = [(x-x_0)^2 + (y-y_0)^2]$ in Fig. 1(d) and t is time. Whereas in problems of beam fusion, the fusion event especially in case of the discretized step D_i will be of an instantaneous nature where time intervals of a small fraction of a second are usual. In this case, heat transfer in the target in such short time intervals has to be determined. Here, it is reasonable to assume uniform strength in a source of small length as D_i for conditions of beam heat dissipation. Also, equation (8) has been normalized for a constant value of T and written here to describe the advance F of isothermal T during heat transfer in the solid metal

$$F = \left[\frac{Q_0}{4\pi^2 T}\exp(-R_0^2/4k_0 t)\right]^{1/2}. \tag{9}$$

In the following, equation (9) has been further developed through numerical analysis, in order to suit the cases of source travel as well as melting. Here, in case of relative-transverse movement between beam and target, F is proportional to half power of parameter V' which is equal to (Vt_i). For this condition, equation (9) modifies to

$$F_i = \left[\frac{Q_0 V'}{4\pi^2 x_0 T}\exp(-R_0^2/k_0 t)\right]^{1/2} \tag{10}$$

where F_i is the advance of the isothermal T in time t_i during the traverse of the beam in the target and x_0 is a unit distance. Here, equation (10) takes into account the enhanced spread of isothermals in the travel direction as a result of source travel.

Now, considering an intense beam which produces instantaneous melting in the metal, the advance (f) of the melting-point isothermal (T_m) must be determined. In this case, in view of absorption of latent heat of fusion (L_m), the advance of isothermals is expected to be slower as compared to the case of heat flow without fusion for similar conditions of heat input. Here, equation (10) modifies to give the advance f of the melting-point isothermal T_m during fusion by an electron beam and under conditions of travel, as

$$f = \left[\frac{f_0 q_0 V'}{4\pi^2 x_0 T_m}\exp(-R_0^2/4k_0 t)\right]^{1/2} \tag{11}$$

where $q_0 = Q_0$ for the intense beam case. In this equation, the influence of the latent heat of fusion L_m, is incorporated through the dimensionless parameter f_0 which is defined below in terms of beam parameters and metal properties

$$f_0 = \left[\frac{K_e}{c_e + L_e}\frac{r_0}{S}\right]^{1/2} \tag{12}$$

where K_e, c_e and L_e are energy parameters which depend on K, c, and L_m respectively, r_0 is the beam spot half width, R_0 is an interface distance parameter which is written as

$$R_0 = \beta_0 R_i. \tag{13}$$

Here β_0 is a dimensionless parameter which is equal to $[(r_0/x_0)(1+\cos\phi)]^{-1/2}$ where ϕ is the beam angle. Here β_0 takes into consideration the effect of beam density on fusion. For example, for a given value of R_i, a small r_0 and large ϕ means a highly collimated beam (e.g. focused spot). In this case, β_0 will be large and so the advance of the isothermals will be slow. That is, this gives rise to a more localized effect. But in the case of large r_0 and small ϕ, β_0 will be small which gives rise to comparatively large values of f for the given values of R_i and beam quantities. Hence the present model, fits well to fusion by focused beams (high density) as well as low density (uncollimated case) beams. R_i in equation (13) is the isothermal distance and is equal to $[(x-x_0)^2+(y-y_0)^2]^{1/2}$ in case of lateral melting, but equals S in z_i melting. For the special cases of growths in the x–z and y–z planes, R_i is directly given either by $X_{(i,k)}$ or $Y_{(i,k)}$, respectively, which are written as

$$\begin{aligned} X_{(i,k)} &= r_0 + \sum_{k=i}^{j} k^x_{(i,l)} \\ Y_{(i,k)} &= r_0 + \sum_{k=i}^{j} k^y_{(i,l)} \end{aligned} \tag{14}$$

where k denotes all the growth steps valid for a given step i, and $k^x(i, l)$, and $k^y(i, l)$ are equal to f and are described by equation (11) and illustrated in Fig. 1(a). Whereas, the temperature, T, at the key-hole base as explained above is expected to be higher than T_m. In view of this, z_i in this case is obtained as (T/T_m) times of f that is given by equation (11). Here, by superposing the results from equation (11) for all D_i steps, the total fusion spreadings in the x- and y-directions, are obtained over the full depth. Similarly, the same effect along depth (i.e. z-direction) is included in D_i in equation (4).

In case of travel speed V [see Fig. 1(c)], the value of R_i in the traverse direction (i.e. y-direction here) is given as

$$R_i = Y_{(i,k)} - Vt_i. \tag{15}$$

In this case, the isotherm for the case of source travel is tracked by superposing the solutions for a set of discrete line sources which follow one after another. Apart from these in the stationary condition of the source, $V' = [t_i(k_0/\pi)^{1/2}]$. Also, as far as thermal conduction, convection, and movements in melt, are concerned, in general, they tend to destroy temperature gradients in the melt. In this process, part of the beam heat is continuously made available at the melt–solid interface for the onward spread of isothermals and fusion in transverse directions. Whereas isothermal and fusion spreads happen due to thermal conduction in the solid metal, and are described by equation (11).

The thermal-spread theory developed in this section has been generalized to describe fusion in different metals and having extreme values of thermal conductivities. For this purpose, metals are identified to belong to one of the two groups of thermal conductors in the present study. Accordingly, in the first group, belongs all metals having K values less than $K_0 = 100\ \mathrm{J\ m^{-1}\ K^{-1}\ s^{-1}}$, and the second category contains metals having K values higher than this. Here, K_0 is an arbitrarily chosen limit above which thermal conductivity effects become significant. Also, according to this characterization, in view of small values of K in the first group, the advance of the fusion growths in these metals are assumed to move in step with its isothermal-boundary advance. As a matter of fact, the thermal-spread theory described above gives an exact description of fusion growths in these metals directly. A typical example for such metals will be steel. Whereas in good thermal conductors (i.e. $K > K_0$), the fusion zone will be restricted to a small fractional part of the isothermal envelope, say only about $[(K_0/K)^{1/2}]$ part of f which is given by equation (11). In this manner, isothermals, fusion and their behaviours in metals upon beam irradiation are solved here in a simple model. The added advantage of this model is that the actual beam interactions and fusion can be easily visualized in this. Also, it is convenient to apply this model to computer simulation through which actual fusion profiles are determined here.

4. COMPUTATIONS OF HEAT DISSIPATION

The fusion model described presently, has also been solved in a computation scheme given in Fig. 1(e), to study the fusion behaviour in different metals. For this, the initial temperature conditions in metal are assumed to be $T = T_0$ and $\nabla T = 0$. And on beam irradiation T increases and fusion sets in. For this case, time interval t_i has been relaxed with respect to fusion and its growths, and with the beam energy deposited in the metal. Here, except for the first few time intervals (t_i) from beam-on, the beam deposition is happening inside the key-hole [3, 6, 11] and hence surface reflections are generally neglected in the case of deep penetration. In these cases, the beam energy deposited in the metal has been balanced and used according to the following approximations

$$H_D(i) = \pi r_0^2 D_i q \tag{16}$$

$$Q_{(i,l)} = \pi[X^2_{(i,k)} - X^2_{(i,k-1)}]D_i q \tag{17}$$

where

$$q = \rho[c(T_m - T_0) + L_m]. \tag{18}$$

Whereas, for relative traverse speed condition (Fig. 1(c)), equation (17) modifies to

$$Q_{(i,l)} = \pi\gamma_0[Y^2_{(i,k)} - Y^2_{(i,k-1)}]D_i q \tag{19}$$

where γ_0 is a fractional melt part generated in any single step as a result of the travel condition. Moreover, wherever a higher temperature (T) in the melt is present,

a heat content q_m is used in place of q

$$q_m = q + \rho_T c(T - T_m). \quad (20)$$

Here for average penetrations of about 50 mm, since temperature T is very much less than the boiling point T_B, evaporation rates are typically small (of the order of 10^{-10} kg s^{-1}) as compared to melting rates of more than 0.01 kg s^{-1}. As a matter of fact, latent heat of evaporation L_v has been neglected here. However, in case of rapid boiling in the melt [13], the evaporative term has to be included in equation (16) which for this case modifies to

$$H_D(i) = \pi r_0^2[D_i q_m + m_0 t_i L_v] \quad (21)$$

where q_m is at $T = T_B$. Boiling in the melt is expected only in case of penetrations of one or two orders higher than the values cited in this study, for metals in general.

Also, as stated earlier, fusion spread in a good thermal conductor is only about $[(K_0/K)^{1/2}]$ part of the isothermal advance. Hence for this case, equation (17) has been modified and used as follows

$$Q_{(i,l)} = \pi D_i[X^2_{(i,k)} - X^2_{(i,k-1)}] \times \left[\frac{K_0}{K} q_m + \left(1 - \frac{K_0}{K}\right) \rho c(T_m - T_0)\right]. \quad (22)$$

In a similar manner, equation (19) has also been modified and used. Whereas for a beam deposition time of t', energy deposited (Q) in the metal will be equal to Wt'. Hence $H = Q$ is the condition to arrive at beam-fusion results under given conditions.

In the computations, the value of t_i has been always assumed from an earlier step and thereafter corrected through relaxations. Here, in the first time interval t_1, the electron beam penetrates a depth S and causes melting during which thermal-conduction melting occurs in a further depth z_1 in the beam direction. Also, thermal-conduction melting sideways is also determined using equation (11). In this case, time t_0 to melt depth S, provides the initial assumed value for t_1 which is corrected thereafter as $t_1 = [H_D(1) + H_1]/W$ and used further to correct the values of z_1 and f. From these, fusion depth in the first step $D_1 = S + z_1$ and melt half width $X_{(1,1)} = r_0 + x_{(1,1)}$ for $K < K_0$; and $D_1 = S + z_1 (K_0/K)^{1/2}$ and $X_{(1,1)} = r_0 + x_{(1,1)} (K_0/K)^{1/2}$ for $K > K_0$. From here, the calculations, proceed to the second step, and then to the third, and so on. In this manner, the total fusion depth $h = \sum_{i=1}^{j} D_i$ which is in j steps and in a beam-on time t'. Also, lateral-melt growths as a function of local melt width and time, are determined and added to the melt width continuously. In this manner, the maximum beam penetration and the fusion profile in a given beam-on time t' could be obtained. From here, in case of source travel, calculations move on to the next traverse time interval t', and then to the next, and so on. In these cases, the beam impact level on the solid metal, and melt widths in the travel direction, given by equation (15) at the beginning of each t', are described to start with, and then fusion calculations allowed to continue. In this manner, the beam is taken over the target through a series of traverse time intervals (t') whereby a continuous fusion profile by the beam is obtained for the case of source travel. The calculations proceed further to check onset of steady state before terminating the computations. Hence, through this scheme, a complete description of beam fusion and penetration could be obtained.

In the case of temperature in the melt, an average value of this is found to be appropriate in the calculations. For this purpose, a knowledge about the temperature at the key-hole base is necessary as this is the maximum temperature present in the melt. In the present study, this temperature has been determined through pressure balancing in the key-hole using equation (3) transiently. Here, on knowing the vapour pressure at the base, the corresponding temperature is derived using vapour pressure data from the literature [14]. Moreover, in order to obtain a consistent value of the key-hole base temperature (T), some relaxation of variables P_v, ρ_T and σ_T with T is found to be necessary. In these cases, the thermophysical properties of metals [15, 16] and melts [17] which are used in the present calculations, are tabulated in Tables 2(a) and (b). Also, as far as the values of c and K are concerned, average values [2] of these have been found to be adequate in general.

5. RESULTS AND DISCUSSIONS

The values of heat contents in various metals and in their melts, and at different temperatures are presented in Table 3. Moreover, the values of (f_0/T_m) and β_0 which are evaluated in equations (11)–(13) and used here, are also given in this table. Using these, advance of the melting point isothermal in different metals are determined for various conditions. From these, results

Table 2(a) Metal properties [15, 16]

Metal	ρ (kg m^{-3})	c at 293 K (J kg^{-1} K^{-1})	$\frac{dc}{dT}$ (J kg^{-1} K^{-2})	K at 293 K (10^2 J m^{-1} K^{-1} s^{-1})	$\frac{dK}{dT}$ (10^{-1} J m^{-1} K^{-2} s^{-1})	T_m (K)	L_m (kJ kg^{-1})
Al	2700	920	0.46	2.39	−0.5	933	388.04
SS	7900	502	0.475	0.152	0.1298	1783	300
Cu	8930	386	0.084	3.935	−1.884	1356	204.779

Table 2(b). Melt density and surface tension [17]

Metal	Melt density (ρ_m) at T_m ($kg\,m^{-3}$)	$\frac{d\rho}{dT}$ ($kg\,m^{-3}\,K^{-1}$)	Surface tension (σ_0) at T_m ($N\,m^{-1}$)	$\frac{d\sigma}{dT}$ ($10^{-4}\,N\,m^{-1}\,K^{-1}$)
Al	2380	−0.114	0.914	−3.5
Fe	7010	−0.119	1.872	−4.9
Ni	7770	−0.142	1.778	−3.8
Cu	7990	−0.100	1.36	−2.1
Ag	9330	−0.097	0.903	−1.6

for aluminium, stainless steel and copper are compared in Fig. 2 as a function of fusion depth (h) for quasi-stationary to steady-state conditions in the travel mode. This comparison indicates the nature of metal response to intense heating and thermal conduction. In addition, the plots reveal that the growths increase with h and attain fixed values at steady state. Here for the case of z_i, time t in the exponent in equation (11) equals t_i. But in the case of $y_{(i,l)}$, $t = \sum_{i=1}^{j} t_i$. This difference in t values accounts for the differences in the z_i and $y_{(i,l)}$ values (as shown in this figure) at the beginning of the penetration. Also the value of t in z_i approaches that in $y_{(i,l)}$ as steady state is neared and thereafter both the time variables assume an average value as required by the steady-state condition. Whereas higher values of z_i towards steady state, are attributed to an effect of the (T/T_m) factor in the growth equation. Also among the metals studied here, growth in stainless steel can be seen to be lower than those in copper. However, stainless steel being a poor thermal conductor, its isothermal growths given in Fig. 2 have been directly used as the fusion growths in this metal. Fusion growths in copper are only about $[(K_0/K)^{1/2}]$ part of its isothermal growths. In view of these, actual fusion spreading in stainless steel in effect is comparatively larger than that in copper for given conditions.

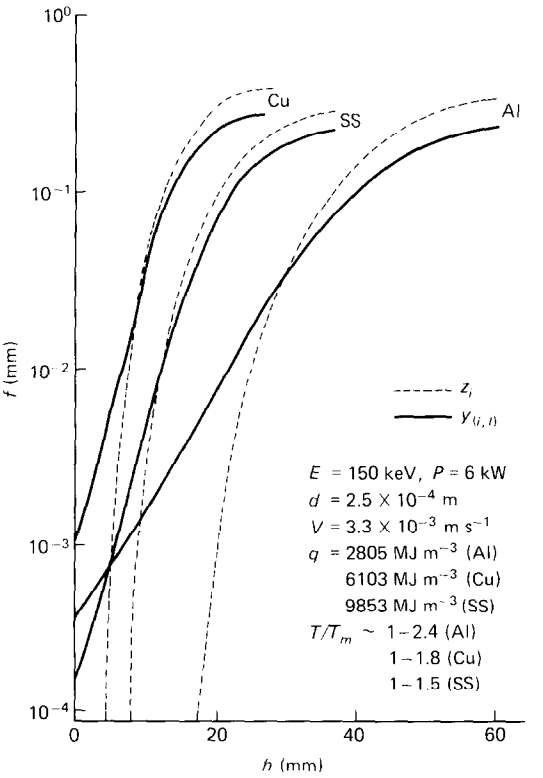

FIG. 2. Transient and steady-state fusion growths in different metals with source travel.

As far as the heat term $Q_{(i,l)}$ in equation (6) is concerned, its variation in various metals are seen to be characteristic of the metals. In this case, variation of $Q_{(i,l)}$ for increasing steps of penetrations in aluminium, are plotted against h in Fig. 3 for the quasi-stationary condition. A comparison of $Q_{(i,l)}$ in different metals for a given penetration step is also obtained in this figure which shows that higher values of $Q_{(i,l)}$ are needed in copper for given conditions while aluminium needs small $Q_{(i,l)}$. Also, variations of H_i with h in the given metals for quasi-stationary to steady-state cases of travel mode, are illustrated in Fig. 4. In this figure, H_i values during the quasi-stationary state in the first traverse-time interval of t', are given by the dashed

Table 3. Typical values of heat variables

Metal	q ($MJ\,m^{-3}$)	q_m at an arbitrary temperature $T = 2080$ K ($MJ\,m^{-3}$)	r_0 (mm)	ϕ (deg.)	β_0 (10^2)	S (mm)	$\frac{f_0}{T_m}$ ($10^{-6}\,K^{-1}$)
Al	2805	5602	0.25	30	0.4629	0.195	1.019
Cu	6103	9326	0.25	30	0.4629	0.069	2.275
SS	9853	11 547	0.25	30	0.4629	0.076	0.4708

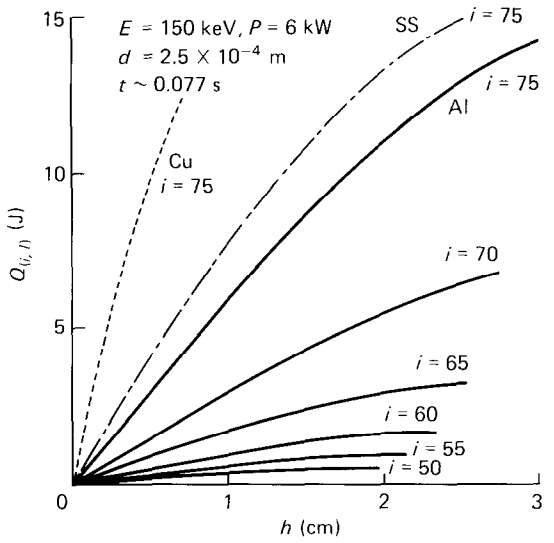

FIG. 3. $Q_{(i,I)}$ in equation (6) vs penetration depth h for stationary case in aluminium and comparison with different metals.

curves, while, the solid curves give the values from the second interval of t' onwards up to steady state. Here, at the end of the first t', as the beam is moved to the next traverse step due to travel, the beam is located at an upper level (i.e. a smaller h which is given by the x-intercept of the solid curve) in the metal. In this location of the beam, the lateral fusion tends to grow only on the side of source travel. In view of these, the value of H_i at the beginning of the second t' is zero which increases again as h increases through successive traverse steps to steady state. Whereas, the dashed curve alone as presented in this figure, describes a given stationary source case as well. In addition, isothermal (T_m) boundaries $Y_{(i,k)}$ in different metals are obtained from quasi-stationary to steady state of travel, and are plotted in Fig. 5.

Apart from these, the results from calculations of key-hole base-temperatures are plotted in Fig. 6 as a function of key-hole depth. Here, the temperature profile down the key-hole will be defined by the two extremes, namely, temperature at the key-hole opening (around the melting point), and the maximum temperature which is at the key-hole base. In Fig. 6, differences in temperatures and its variations with key-hole depth for different metals and given conditions, are attributed in general to extreme differences in surface tension properties of metals and those in their variations with temperature, respectively. In this study, these temperatures have been applied for the determination of z_i growths and for the estimation of the average temperature in the melt.

In addition to these, beam penetrations have also been determined from the fusion model described above, for various electron energies and power in the beam, travel speeds, different metals, and varying focusing conditions of the beam. In these cases, there is an uncertainty about the exact temperature in the melt. Here the temperature in the melt is always higher than the melting point but lower than the temperature at the

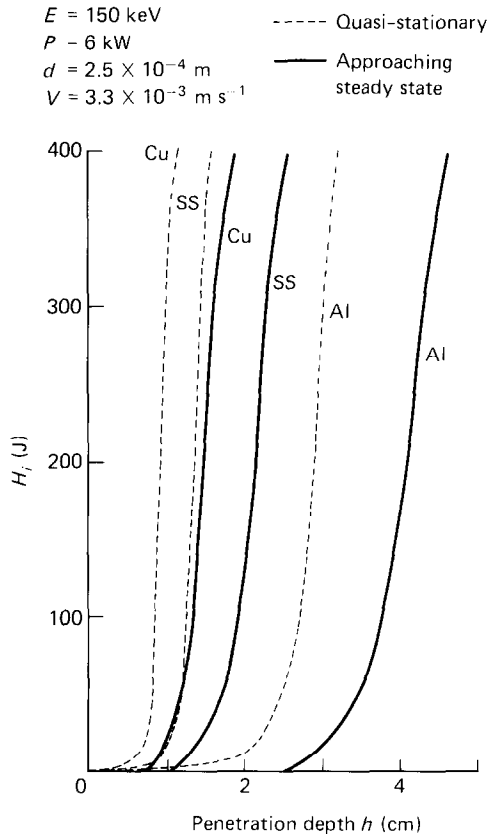

FIG. 4. H_i in equation (6) vs penetration h in different metals during dynamic state of target travel.

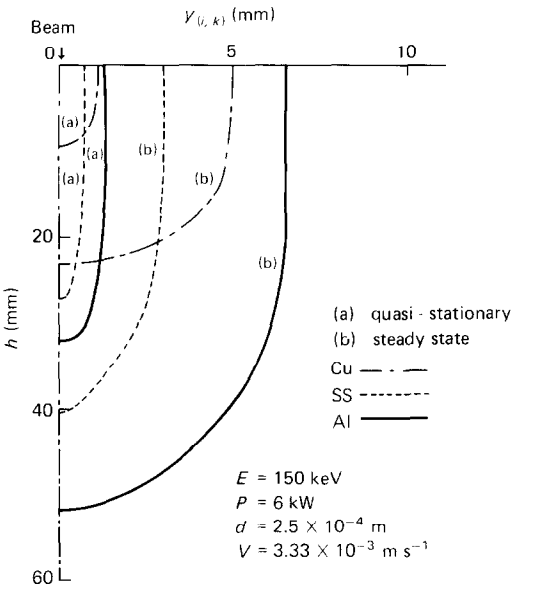

FIG. 5. Calculated values of $Y_{(i,k)}$ vs fusion depth for travel case in different metals.

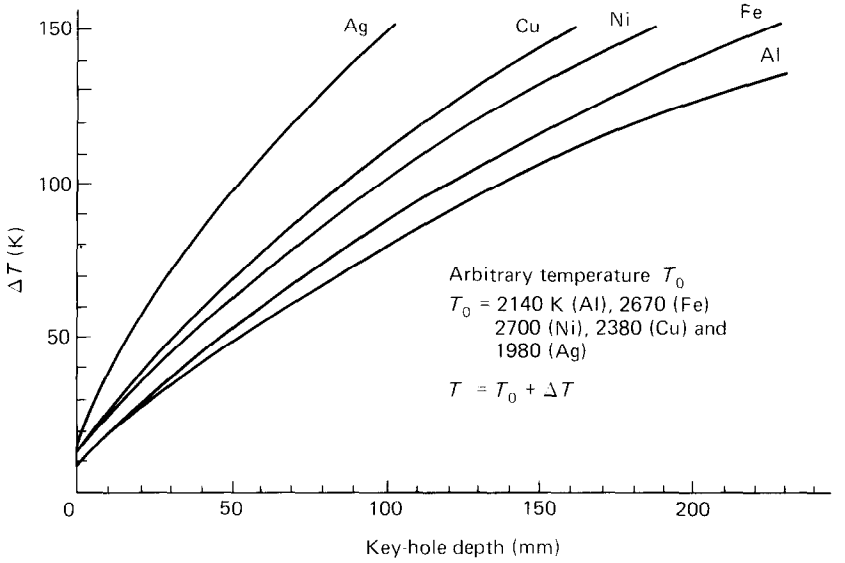

FIG. 6. Key-hole depth vs temperature at its base for a general case with $d = 1 \times 10^{-4}$ m.

key-hole base which in the present case is the maximum temperature predicted in the melt. Here for conditions under beam interactions, an average temperature in the melt can be assumed in calculations, the exact value of which, however, is difficult to predict in actual situations. In view of this, fusion penetrations were computed separately for the two fixed temperatures in the melt (i.e. melting point and temperature at the key-hole base) for a given case. Accordingly, results from these two extreme temperatures, provide penetration values and their range of variation with temperature. Hence, once the temperature in the melt is exactly known, the actual penetration value can be obtained from this. In this case, the extent of error possible in h against temperature variation is estimated to be about $(5.6 \times 10^{-9}\ \text{V})\ \text{mK}^{-1}$ per kW of power in stainless steel.

From the calculations carried out in this manner, results in stainless steel for an electron energy of 100 keV and varying beam currents and travel speeds, are plotted in Fig. 7. In this case, the temperature at the key-hole base for a hole depth of 50 mm which is about the average depth of interest in practice, is used as the maximum temperature which is about 2700 K. From the figure it can be seen that penetration values for a beam current of 30 mA and a travel speed of $3.33 \times 10^{-3}\ \text{m s}^{-1}$, range from 23.6 to 18.7 mm for the melting point (T_m) and $T = 2700$ K assumptions, respectively. Also in the same figure is given a comparison of h at different electron energies, by including the results at another electron energy of 150 keV. In this case and also in the succeeding figures, penetration results from the assumption of the melting point alone are given for comparing the influence of various parameters. It can be seen from Fig. 7 that fusion penetration at 150 keV for given conditions is higher than that at 100 keV. This is in view of electron residual range S being large at a higher energy. Whereas Fig. 8 gives the fusion results in various metals, and shows that, of the metals investigated here, penetration in aluminium is maximum and that in copper is minimum. Moreover, Fig. 9 illustrates the penetration results for varying focusing conditions of a given beam of different power levels. It can be seen from this figure that, it is possible to generate enhanced penetrations in metals by simply focusing the electron beam to a high density. This is a significant advantage of electron-beam heat transfer.

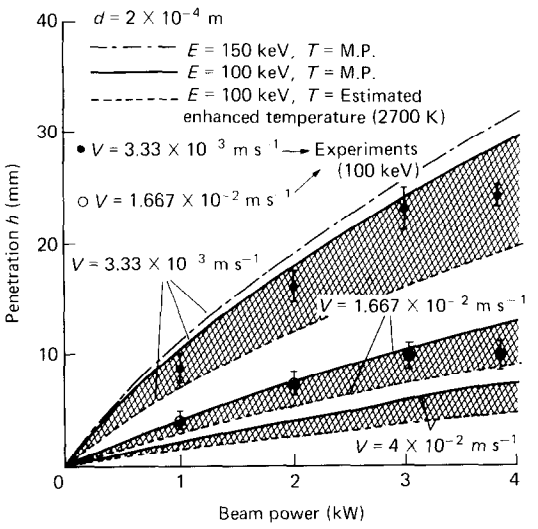

FIG. 7. Fusion penetrations vs beam power in stainless steel 304 targets with travel speed.

6. EXPERIMENTAL RESULTS

The beam-fusion model presently developed has been validated through experiments of deep-

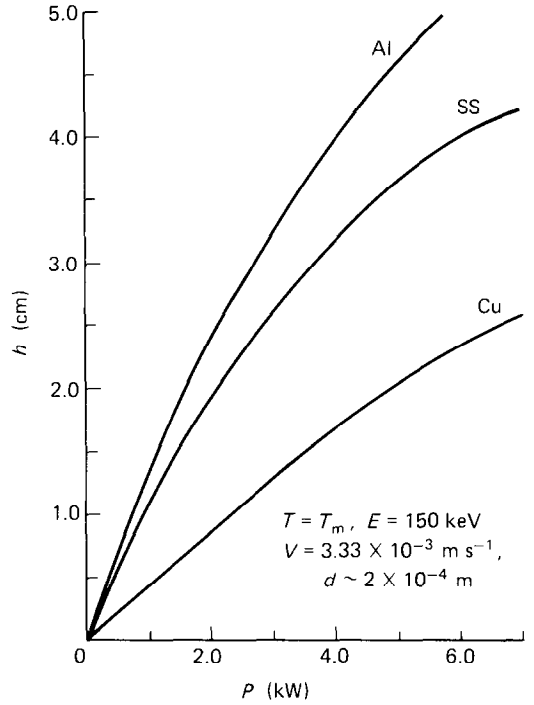

FIG. 8. Computed fusion penetrations in different metals.

penetration fusion in metals by using focused beams of moderate energy (100 keV) and powers (a few kilowatts) in this study. In these experiments the beam was made normally incident on the target metal which was moved laterally at a travel speed as applied in theory.

The experimental set-up [18] used for this study, consists of an electron gun which generates an electron beam of a power level as required, a focusing lens to collimate the beam onto the target, and a work-table for target movements inside vacuum. Also, in the present

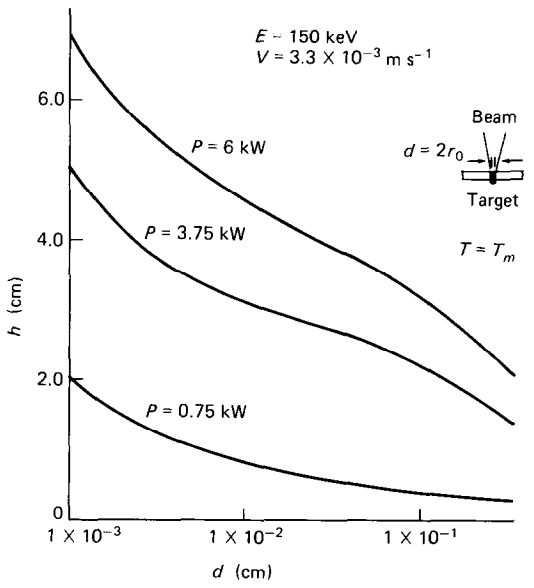

FIG. 9. Fusion penetrations with different power densities and for given conditions in stainless steel.

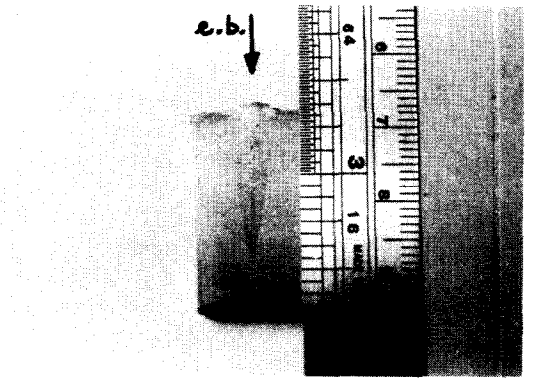

(a)

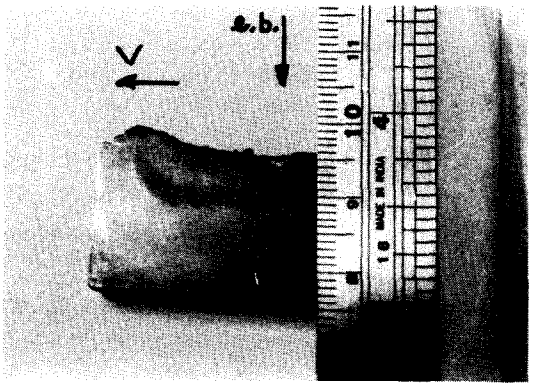

(b)

FIG. 10.(a) Photograph of the section of a beam-fusion profile: $E = 100\,\text{keV}; P = 4\,\text{kW}; V = 5 \times 10^{-3}\,\text{m s}^{-1}$.(b) Photograph of the section of a fusion trail in the case of source travel: $E = 100\,\text{keV}; P = 2\,\text{kW}; V = 5 \times 10^{-3}\,\text{m s}^{-1}$.

set-up, the electron gun has a triode geometry in which the cathode electrode is a tungsten V-filament, the control electrode is of hemispherical design, and the anode is cylindrical having a funnel-shape. Using this set-up, beam-fusion studies on various metals were conducted, and a number of samples were obtained for investigations.

The fusion zone in these samples were sectioned and studied further. In these cases, sections were made in a plane perpendicular to the target-travel direction but containing the beam direction. The chemically-polished surfaces of these sections visually describe the fusion zones in these. Of the sections studied in this manner, the photograph of a typical fusion profile is presented in Fig. 10(a). It can be seen from this figure that the beam-fusion profile in metals in practice is identical to the one which is predicted by theory in Fig. 1(a). In addition, fusion development in the plane containing the travel direction and beam, was also investigated experimentally for the beam-on stage up to the beam-off time. The photograph in Fig. 10(b) shows a typical view of such a fusion section in the metal. In reality, this fusion zone conforms to the predicted behaviour of fusion development during travel speed in Fig. 1(c).

In addition, in the experiments, fusion depths in different metals were determined for varying conditions of beam and travel speed. From these, the results in the case of stainless steel 304 using a beam energy of 100 keV and powers up to a few kilowatts, and at two travel speeds are plotted in Fig. 7 along with the theoretical plots. In this case, the variations in fusion penetrations as indicated on the experimental plots, are due to some uncertainties [19] in experimental conditions such as slight change in travel speed, that in focusing of the beam, etc., from experiment to experiment. Apart from these, it can be seen that the measured penetrations fall well within the two extremes predicted by theory. Hence it is evident that by and large there is reasonable agreement between measurements and calculations.

Apart from these, the present model has also been applied to fusion of dissimilar metals. In dissimilar-metal welding, fusion behaviour of the metals may be of extreme nature (for e.g. copper–stainless steel combination), for which the uniform-beam incidence mode on the two metals cannot be employed straight away as we do for similar metal joints. Whereas, the ratio of beam inputs on the two metals have to be so adjusted to give equal fusions of the two metals which facilitate proper joining of the two. In these cases, Figs. 2–5 are of routine help, and have been applied in dissimilar-metal welding experiments, results of which will form the subject of another paper.

7. CONCLUSIONS

Through this study, an adequate model of beam-energy transfer and fusion in metals has been developed and adapted to numerical computation. In the transient stage of key-hole development, since the beam is delivering energy at different depths in the metal, the present model is a close physical representation of this. The same is true of the steady state also. Hence, this model provides a good description of both transient as well as steady-state fusion in deep penetration. Here, by including the transient effects, in addition to understanding the metal response under these conditions, a steady-state model which in itself is consistent with metal response both to the beam as well as to heating, is provided by this study. In these respects, the present model is an improvement over the other models. Also the influence of temperatures in the melt for the purpose of deep penetration could be established. In addition, temperature-enhanced spreading of fusion by thermal conduction has been described. Accordingly, the influence of thermal conductivity on fusion has been predicted in various metals through computations. In this case, two groups of metals depending on their K values have been identified. Of these in good thermal conductors, a proper distinction could be made between the melting-point isothermal boundary and fusion boundary in general. Whereas in poor heat conductors, the two more or less overlap. The observed results of fusion profile, penetration, etc. validate the theoretical model presented in this study.

Acknowledgements We are thankful to Shri C. Ambasankaran for his interest in this work. We appreciate the help and discussions from a number of colleagues of this establishment. Further, we would like to thank the referees for their critical comments and suggestions which have helped us in improving the quality of the paper.

REFERENCES

1. H. Schwarz, Mechanism of high power-density electron beam penetration in metal, *J. Appl. Phys.* **35,** 2020–2029 (1964).
2. D. T. Swift-Hook and A. E. F. Gick, Penetration welding with lasers, *Welding J.* **52,** 492S–499S (1973).
3. P. G. Klemens, Heat balance and flow conditions for electron beam and laser welding, *J. Appl. Phys.* **47,** 2169–2174 (1976).
4. J. G. Andrews and D. R. Atthey, Hydrodynamic limit to penetration of a material by a high-power beam, *J. Phys. D: Appl. Phys.* **9,** 2181–2194 (1976).
5. N. D. Malmuth, Temperature field of a moving point source with change of state, *Int. J. Heat Mass Transfer* **19,** 349–354 (1976).
6. N. Rykalin, A. Uglov and A. Kokora, *Laser Machining and Welding* (translated by B. Glebov), p. 78, pp. 120–126. MIR, Moscow (1978).
7. Y. Sharir, A. Grill and J. Pelleg, Computation of temperatures in thin tantalum sheet welding, *Metall. Trans.* **B11,** 2, 257–265 (1980).
8. T. Vijayan, Study of heat and mass transports in metals under electron-beam interactions, Ph.D. thesis, University of Bombay, India (1982).
9. R. Shimizu and K. Murata, Monte Carlo calculations of the electron-sample interactions in the scanning electron microscope, *J. Appl. Phys.* **42,** 387–394 (1971).
10. R. Bakish, *Introduction to Electron-beam Technology*, p. 365. Wiley, New York (1962).
11. A. H. Meleka, *Electron-beam Welding: Principles and Practice*, pp. 85–91. McGraw-Hill, New York (1971).
12. H. S. Carslaw and J. C. Jaeger, *Conduction of Heat in Solids*, p. 256. Oxford University Press, London (1959).
13. J. G. Andrews and D. R. Atthey, *J. Int. Math. Applic.* **15,** 59–72 (1975).
14. R. E. Honig, Vapour pressure data, *R.C.A. Rev.* **18,** 195–204 (1959).
15. C. J. Smithells, *Metals Reference Book*, Vol. III, pp. 685–707. Butterworths, London (1967).
16. W. M. McAdams, *Heat Transmission*, pp. 445–447, McGraw-Hill, Japan (1954).
17. Sylvan Z. Beer, *Liquid Metals*, pp. 186–191. Marcel Dekkar, New York (1972).
18. T. Vijayan and V. K. Rohatgi, Transport of high-energy and high-power electron beams in a tetrode gun, *J. Phys. D: Appl. Phys.* **11,** 2157–2168 (1978).
19. J. G. Andrews and D. R. Atthey, The response of a weld pool to perturbations in power, *Int. J. Heat Mass Transfer* **22,** 1533–1538 (1979).

COMPORTEMENT PHYSIQUE PENDANT LA FUSION PAR BOMBARDEMENT ELECTRONIQUE DU TRANSFERT THERMIQUE ET DE LA PROFONDEUR DE PENETRATION DANS LES METAUX

Résumé—Un modèle de fusion simple et de pénétration dans les métaux est décrit en tenant compte des interactions du faisceau d'électrons et du transfert d'énergie. Dans ce modèle, les électrons pénètrent à la profondeur S et provoque la fusion, pendant que la conduction thermique prolonge la fusion à la profondeur z_i. Dans le premier pas de fusion discrétisée, la profondeur de fusion est $D_1 = S + z_i$ et la profondeur totale de fusion en j pas est $h = \sum_{i=1}^{j} (S + z_i)$. La conduction thermique à partir d'une ligne source de la surface au pied de la cavité cause une fusion latérale. En général, le conduction de fusion f est donnée par

$$f = \left[\frac{f_0 q_0 V'}{4\pi^2 x_0 T_m} \exp\left(-R_0^2/k_0 t\right) \right]$$

où f_0 est la variable adimensionnelle dépendant du métal et du faisceau, q_0 et V' sont les paramètres de la puissance et du trajet de la source, x_0 une distance unitaire, T_m la température de fusion, R_0 une distance variable et $k_0 = K/\rho c$ la diffusion thermique avec k conductivité, ρ masse volumique et c chaleur massique. Pour les métaux avec $K > K_0$ ($= 100$ W m^{-1} K^{-1}), z_i et f sont réduits par $(K_0/K)^{1/2}$ à cause des pertes thermiques à grande échelle. Par ce modèle, les profils de fusion et les pénétrations pour des conditions variées de faisceau et de métaux sont étudiés à travers des calculs numériques et sont validés par des expériences.

DAS PHYSIKALISCHE VERHALTEN DES WÄRMEÜBERGANGS UND DER TIEFEINDRINGUNG BEI DER ELEKTRONENSTRAHL-FUSION IN METALLEN

Zusammenfassung—In diesem Bericht wird ein einfaches Modell vorgestellt, das die Fusion und die Tiefeindringung bei der Wechselwirkung und bei der Energieübertragung von Elektronenstrahlen beschreibt. In dem Modell durchdringen die Elektronen im Strahl eine Tiefe S und verursachen dort das Schmelzen, wobei zusätzliches Schmelzen infolge Wärmeleitung in der weiteren Tiefe z_i in Strahlrichtung auftritt. Daher wird im ersten diskretisierten Fusionsschritt die Fusionstiefe $D_1 = S + z_1$ erreicht, und die gesamte Fusionstiefe beträgt nach j Schritten $h = \sum_{i=1}^{j} (S + z_i)$. Ebenso bewirkt die Wärmeleitung aus einer linienförmigen Quelle von der Oberfläche zum Boden des Hohlraums seitwärtiges Schmelzen. Allgemein kann der Schmelzparameter f aufgrund der Wärmeleitung wie folgt beschrieben werden:

$$f = \left[\frac{f_0 q_0 V'}{4\pi^2 x_0 T_m} \exp\left(-R_0^2/k_0 t\right) \right].$$

Hierin sind f_0 eine dimensionslose Variable, die von Strahl und Metall abhängt, q_0 und V' sind Quellstärke- und Quellweg-Parameter, x_0 eine Einheitslänge, T_m die Schmelztemperatur, R_0 eine Längenvariable, $k_0 = K/\rho c$ die Temperaturleitfähigkeit, K die Wärmeleitfähigkeit, ρ die Dichte des Metalls und c dessen spezifische Wärmekapazität. Das seitliche Schmelzen in aufeinanderfolgenden Stufen summiert sich von der ursprünglichen zur endgültigen Schmelzbreite auf. Für $K > K_0$ ($= 100$ J m^{-1} K^{-1} s^{-1}) verringern sich die Schmelzgrößen z_i und f mit $(K_0/K)^{1/2}$ infolge thermischer Verluste. Fusionsprofile und Eindringtiefen wurden für zahlreiche Bedingungen bezüglich des Strahls und des Metalls durch numerische Berechnungen mit dem vorliegenden Modell untersucht und durch Experimente belegt.

ФИЗИЧЕСКИЕ АСПЕКТЫ ТЕПЛОПЕРЕНОСА И ГЛУБИННОЕ ПРОПЛАВЛЕНИЕ МЕТАЛЛОВ ЭЛЕКТРОННЫМ ЛУЧОМ

Аннотация—Рассмотрена простая модель глубинного проплавления и энергопереноса в металле при воздействии электронного пучка. В соответствии с предложенной моделью электроны пучка проникают на глубину S, расплавляют в этом месте металл, который за счет теплопроводности расплавляет следующий по направлению луча участок z_i. Следовательно, на первом дискретном шаге глубина проплавления составляет $D_1 = S + z$, а полная глубина проплавления за j шагов равна $h = \sum_{i=1}^{j} (S + z_i)$. Кроме того, за счет теплопроводности от линейного источника, проходящего от поверхности металла до дна полости, происходит плавление в радиальном от источника направлении. В общем случае процесс плавления, обусловленный теплопроводностью, f, можно описать соотношением

$$f = \left[\frac{f_0 q_0 V'}{4\pi^2 x_0 T_m} \exp(-R_0^2/k_0 t) \right]$$

где f_0—безразмерная переменная, характеризующая луч и металл; q_0 и V'—параметры, определяющие мощность источника и его перемещение; x_0—единичное расстояние; T_m—точка плавления; R_0—переменная расстояния; $k_0 = K/\rho c$—температуропроводность; K—коэффициент теплопроводности; ρ—плотность металла и c—удельная теплоемкость. Плавление в радиальном от источника направлении на последующих интервалах времени суммируется с начальной шириной расплава для определения конечной его ширины. Кроме того, у металлов $K > K_0 (= 100$ Дж м$^{-1}$ К$^{-1}$ s^{-1}), величины z_i и f уменьшаются на $(K_0/K)^{1/2}$ из-за крупномасштабных тепловых потерь в окружающую среду. По предложенной модели с помощью численных расчетов исследованы конфигурации расплава для различных пучков и металлов. Результаты расчетов подтверждены экспериментальными данными.